Heliyon 8 (2022) e09373

Contents lists available at ScienceDirect

Heliyon

journal homepage: www.cell.com/heliyon

Research article

New copper(II) μ-alkoxo-μ-carboxylato double-bridged complexes as models for the active site of catechol oxidase: synthesis, spectral characterization and DFT calculations☆

Abhay K. Patel [a], Neetu Patel [a], R.N. Patel [a], Rajendra N. Jadeja [b,*]

[a] Department of Chemistry, Awadhesh Pratap Singh University, Rewa, 486003, India
[b] Department of Chemistry, Faculty of Science, The Maharaja Sayajirao University of Baroda, Vadodara, 390002, India

ARTICLE INFO

Keywords:
Catecholase activity
Bridged copper(II) complexes
SOD activity
DFT calculations

ABSTRACT

A series of four copper(II) μ-Alkoxo-μ-carboxylato double bridged complexes, $[\{Cu_2(L)\}_2](\mu\text{–}O_2C\text{–}CO_2]$ **1**, $[\{Cu_2(L)\}_2(\mu\text{–}O_2C\text{–}(CH_2)CO_2]$ **2**, $[\{Cu_2(L)\}_2(\mu\text{–}O_2C\text{–}CH_2\text{–}CO_2]$ **3** and $[\{Cu_2(L)\}_2(\mu\text{–}O_2C\text{–}C_6H_4\text{–}CO_2]$ **4** (H_3L = 4-bromo-2-((E)-((3-(((E)-5-chloro-2-hydroxybenzylidene) amino)-2-hydroxypropyl) imino) methyl)-6-methoxyphenol and μ-dicarboxylate ions = oxalate, malonate, succinate and terephthalate) have been synthesized and characterized using several physicochemical techniques. The tridentate nature of H_3L is interpreted from IR spectra. The Epr spectra of these complexes are characteristic of the quintet state (S = 2) in central features and the triplet state (S = 1) of these tetranuclear complexes. The electrochemical potential of these complexes was investigated using CV (cyclic voltammetry) and DPV (differential pulse voltammetry). All complexes showed quasi reversible reduction peaks in the cathodic region. To explore the stability of these complexes, quantum chemical parameters like electronegativity, ionization potential, electron affinity, global hardness and softness, and electrophilicity were estimated and discussed. The synthesized complexes have been designed as structural and functional models of the catechol oxidase enzymes to investigate the catecholase activity. Additionally, superoxide dismutase activity data of all complexes have also been evaluated and compared with known SOD mimics.

1. Introduction

Cu(II)-double bridged μ-alkoxo μ-carboxylato complexes have been drawing greater attention as an active side of bio-metalloenzymes [1, 2, 3, 4, 5]. In the context of modelling biological systems, binuclear Cu(II)-centres have an essential functional role in the active site of tyrosinase, hemocyanin, catechol oxidase, etc. Cu-containing proteins [6]. Synthesis and scrutinization for Cu(II)-complexes were done with a catecholase-like functional model [7, 8, 9]. Mechanistic and electrochemical [10] and pH-dependent [11] studies on such binuclear complexes with catecholase activity have been reported in the literature. Catechol to quinone can be done through catechol catalysis, which has greater importance in medical diagnosis [12, 13] (Scheme 1).

Cu(II)-binuclear complexes have drawn considerable interest due to their biological and industrial importance [14]. Current reports give evidence of better efficiency of mononuclear Cu(II)-analogues compare to binuclear complexes [15]. In addition, multinuclear metal complexes are pretty valuable for functional molecule-based material synthon [16]. The synthetic manner of multinuclear complexes is planned at sympathetic chemical or structural aspects that dictate coupling exchange in paramagnetic centres advancing scientific progress [17].

Using magnetic susceptibility measurements, some binuclear Cu(II) complexes with a different diamagnetic bridge can be characterized. Combining carboxylato and oxo groups as bridges can give a coupling yield of weakly antiferromagnetic, strongly antiferromagnetic, and ferromagnetic properties [18, 19].

In the present work, the binucleated Schiff base is formed by condensation 1,3-diamino-2-propanol and substituted salicylaldehyde (3-methoxy-2-bromosalicylaldehyde and 5- chlorosalicylaldehyde). With binucleating ability, these Schiff bases can serve as a bridging alkoxo group. From this binucleating ligand, the bridge in Cu(II) ions the formed between deprotonated alkoxide O-atom and another bridging ligand

☆ This article is a part of the "Coordination compounds" special issue and proceed further.

* Corresponding author.
E-mail address: rjadeja-chem@msubaroda.ac.in (R.N. Jadeja).

https://doi.org/10.1016/j.heliyon.2022.e09373
Received 7 September 2021; Received in revised form 16 November 2021; Accepted 29 April 2022

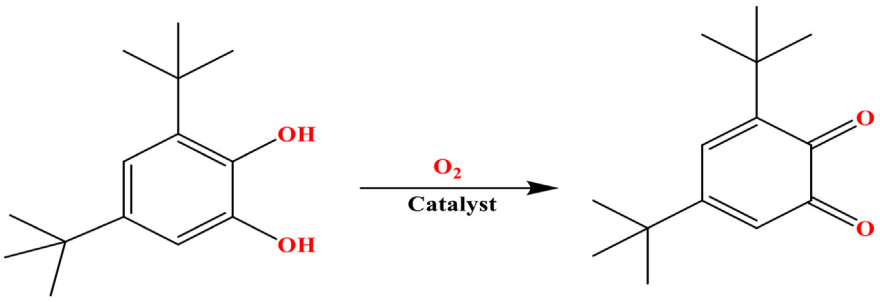

Scheme 1. Conversion of catechol to a quinone.

carboxylate anions such as oxalate, succinate and malonate, and terephthalate ions. Herein, we report four μ-Alkoxo-μ-carboxylate double bridged complexes with four bridging carboxylate anions viz., $[\{Cu_2(L)\}_2][\mu–O_2C–CO_2]$ **1**, $[\{Cu_2(L)\}_2(\mu–O_2C–(CH_2)CO_2]$ **2**, $[\{Cu_2(L)\}_2\mu–O_2C–CH_2–CO_2]$ **3** and $[\{Cu_2(L)\}_2(\mu–O_2C–C_6H_4–CO_2]$ **4**. The Schiff L base is formed by condensation 1,3-diamino-2-propanol and substituted salicylaldehyde (3-methoxy-2-bromosalicylaldehyde and 5-chlorosalicylaldehyde). It possesses a binucleating functionality. Moreover, Cu(II)-ions are bridged by oxalate, succinate, malonate, and terephthalate ions to form tetranuclear species. These complexes are potential functional and structural models mimicking the catechol oxidase copper(II) enzyme active site. QCPs(quantum chemical parameters) calculated at the DFT level was utilized as the physicochemical explanation of complexes to understand the electronic and molecular structures of these synthesised complexes. DFT has various uses in life science, particularly in QSAR (quantitative structural-activity relationships) models development. We also explored the SOD mimetic activity of these complexes.

2. Experimental

All chemicals and solvents were used of analytical grade and used without further purification.

2.1. Synthesis of the schiff base ligand (H_3L)

1,3-diamino-2-propanol (0.90 g, 10.0 mmol) was dissolved in 20 ml methanol and added to a methanolic solution of 5-bromo-3-methoxy salicylaldehyde (0.231 g, 10.0 mmol) and 5-chlorosalicylaldehyde (0.156 g, 10.0 mmol) in 10 mL each. The reaction mixture was refluxed for 3 h and allowed to stand for several days at room temperature. The resulting pale brown crystalline compound was washed with cold ethanol and stored in a calcium chloride desiccator.

Yield; 62%, Anal. Calc. for $C_{18}H_{18}BrClN_2O_4$ (441.71): C, 48.95; H, 4.11; N, 6.34: Found C, 48.50; H, 4.19; N, 6.24 %: ^{1}H NMR (400 MHz, DMSO-d6): δ 13.57 (s, 2H, –OH), 8.52 (s, 2H, –N=CH-). FTIR (KBr, cm^{-1}): 1649 cm^{-1} for ν(C=N).

2.2. $[\{Cu_2(L)\}_2][(\mu–O_2C–CO_2]$ 1

To a stirred methanol (20) mL solution containing H_3L (0.441 g, 1 mmol), sodium oxalate (0.067 g, 0.5 mmol), and triethylamine were added to a methanol solution of copper chlorate hexahydrate (0.740 g, 1 mmol) and 1 h stirring. Then, a green polycrystalline compound was collected by filtration, washed with methanol, and stored in a calcium chloride desiccator.

Yield; 62%, Anal. Calc. for $C_{38}H_{30}Br_2Cl_2Cu_4N_4O_{12}$ (1219.57): C, 37.42; H, 2.48; N, 4.59: Pract. C, 37.38; H, 2.49; N, 4.30 %: FTIR (KBr, in cm^{-1}):1600 cm^{-1} for ν(C=N). ESI-Mass (m/z): 1214.95.

2.3. $[\{Cu_2(L)\}_2\ (\mu–O_2C–(CH_2)CO_2]$ 2

For this complex, in the method of complex **1** preparation, sodium malonate (0.074 g, 0.5 mmol) was used instead of sodium oxalate.

Yield; 62%, Anal. Calc. for $C_{39}H_{32}Br_2Cl_2Cu_4N_4O_{12}$ (1233.59):C, 37.97; H, 2.61; N, 4.54: Found C, 37.50; H, 2.43; N, 4.30 %: FTIR (KBr, cm^{-1}):1569 cm^{-1} ν(C=N). ESI-Mass (m/z): 1228.95.

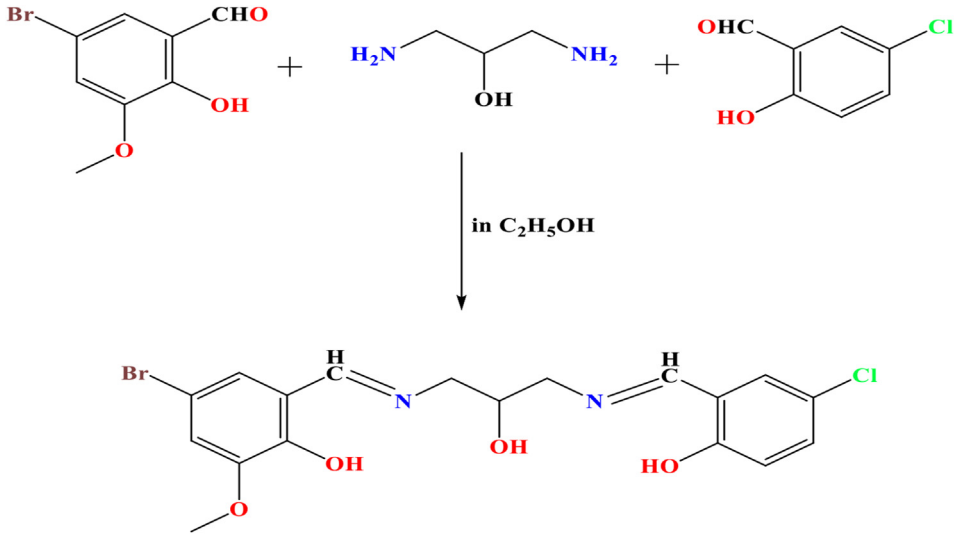

Scheme 2. Synthetic route for schiff base ligand H_3L (= 4-bromo-2-((E)-((3-(((E)-5-chloro-2-hydroxybenzylidene) amino)-2-hydroxypropyl) imino) methyl)-6-methoxyphenol).

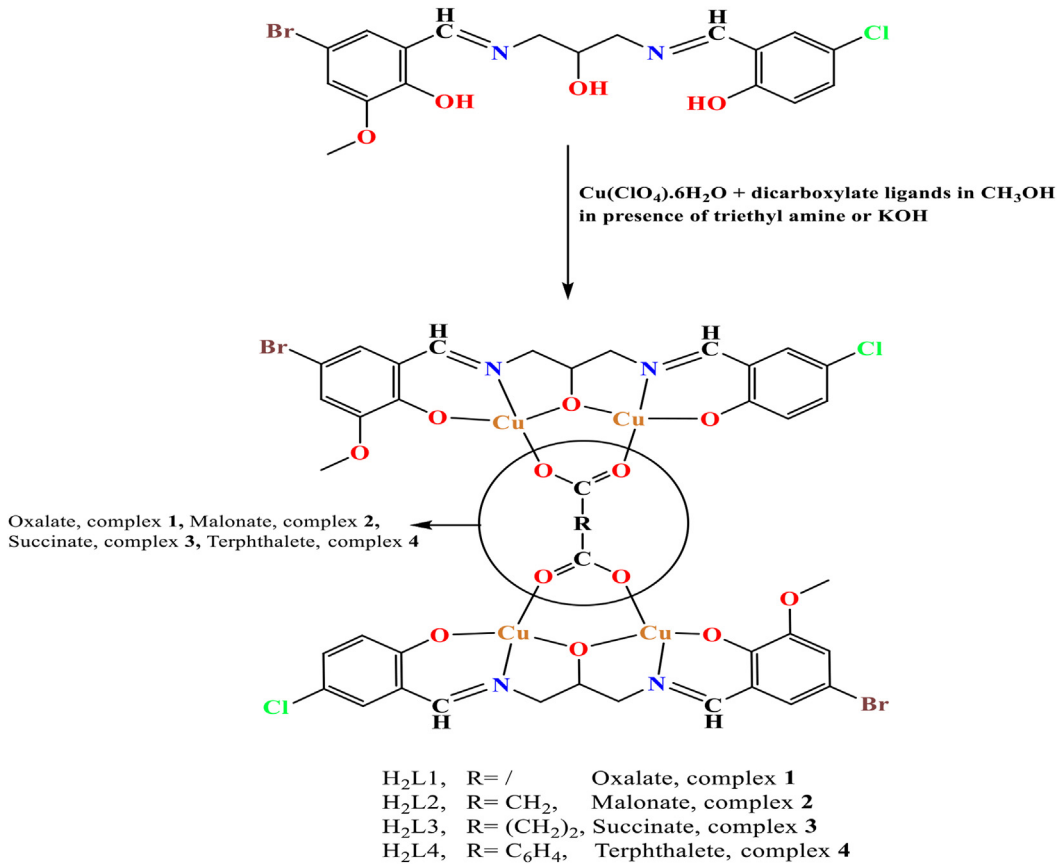

Scheme 3. The synthetic pathway of complexes 1–4.

2.4. $[\{Cu_2(L)\}_2\ (\mu\text{–}O_2C\text{–}(CH_2)_2\text{–}CO_2]$ 3

This complex was synthesized similarly to complex **2** using sodium succinate (0.135 g, 0.5 mmol) instead of sodium malonate.

Yield; 62%, Anal. Calc. for$C_{40}H_{34}Br_2Cl_2Cu_4N_4O_{12}$(1247.62):C, 38.51; H, 2.75; N, 4.49: Pract. C, 38.59; H, 2.49; N, 4.20 %: FT-IR (KBr, in cm^{-1}): 1596 cm^{-1} for ν(C=N). ESI-Mass (m/z): 1242.99.

2.5. $[\{Cu_2(L)\}_2\ (\mu\text{–}O_2C\text{–}C_6H_4\text{–}CO_2]$ 4

To methanolic H_3L solution (0.441 g, 1.0 mmol) terephthalic acid (0.083 g, 0.50 mmol), a methanolic copper(II) perchlorate hexahydrate solution (0.740 g, 1.0 mmol) and KOH (1.0 ml, 1.0 mmol) was mixed. After 2 h stirring and filtration, the filtrate was left for slow evaporation at room temperature. After several days give green crystalline compound appeared that was collected by filtration, washed with methanol, and stored in a calcium chloride desiccator.

Yield; 62%, Anal. Calc. for $C_{44}H_{34}Br_2Cl_2Cu_4N_4O_{12}$ (1295.66):C, 40.79; H, 2.65; N, 4.32: Found C, 40.59; H, 2.49; N, 4.20 %: FTIR (KBr, in cm^{-1}): 1638 cm^{-1} for ν(C=N). ESI-Mass (m/z): 1290.44.

Caution! Perchlorate salts are potentially explosive and should be handled with care. Although, no problems were encountered with the complexes reported herein.

2.6. Physical measurements

Elemental analyses were carried out using an elemental analyzer. IR spectra were obtained through Bruker Spectrophotometer (4000-400 cm^{-1} range, KBr pallets). Electronic spectra measured on Shimadzu model UV-1601 spectrophotometer 10^{-3} DMSO solution. The electrochemistry of complexes was carried out by BAS-100 Epsilon Electrochemistry Analyzer, having a three-electrode system containing cells. Ag/AgCl, Pt wire, glassy carbon, and TBAP (Tetra butyl ammonium perchlorate) were used as reference electrodes, auxiliary electrodes, working electrodes, and supporting electrolytes. ^{1}H-NMR and ^{13}C-NMR analysis of ligand was carried out on FT-NMR spectrometer (BRUKER) in DMSO-d_6 solution, using tetramethylsilane (TMS) as the internal standard chemical shifts (δ) and were reported in δ units downward from TMS. ESR with X-band was obtained through the Varian E-line century series ESR Spectrophotometer. ESI Mass spectrometry was recorded on a XEVO G2-XS QTOF. Electronic conductivities were measured using a Systronics digital conductivity meter (Model TDS-308). X-ray diffraction patterns of polycrystalline samples of complexes were recorded on a Phillips PW 1130 diffractometer with Cu-K_a radiation of wavelength 1.54056 Å. The diffraction angle 2θ was in the range of 0–90°.

2.7. Catecholase activity

At 25 °C, the complexes catecholase–like activity for the air oxidation of 3,5-ditert-butyl catechol (3,5-dtbc) to the corresponding quinone (3,5-3,5-dtbq) was measured spectrophotometrically by using the same procedure as reported in the literature [20, 21, 22]. Using the Michaelis-Menten method, Lineweaver-Burk plots were used to determine kinetic parameters after applying a kinetic treatment.

2.8. Superoxide dismutase (SOD)

As mentioned in the literature, the SOD-like pastime of complexes **1–4** became measured [23, 24, 25, 26].

2.9. Computational calculations

All computational calculations were performed to study geometrical optimization studies by using GAUSSIAN 09 software program [27].

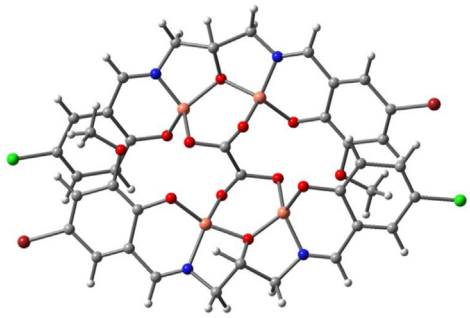

(a)

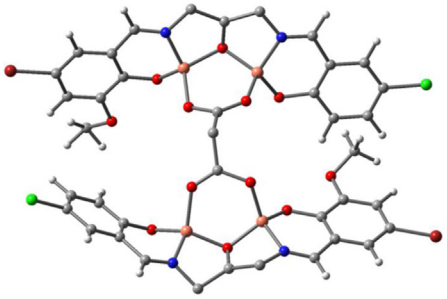

(b)

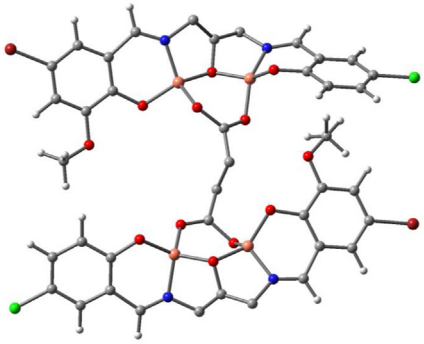

(c)

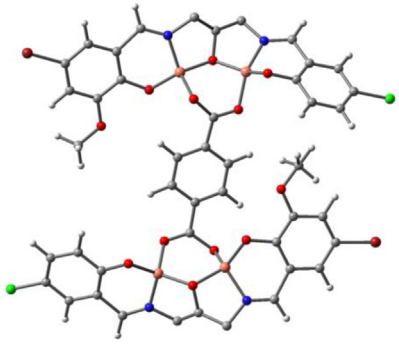

(d)

Figure 1. The conformations of (a) complex **1** (b) complex **2** (c) complex **3** and (d) complex **4** are optimised utilizing DFT.

B3LYP with the 6-31G and LANL2DZ basis set was utilized to improve the molecular geometries of the singlet ground state of complexes [28, 29]. The unrestricted method B3LYP/6–311++G (d,p) GIAO was used to compute theoretical NMR data in the gaseous phase. The structures have been envisioned using a Gaussian view [30].

3. Results and discussion

As indicated in Scheme 2, synthesized ligand H_3L was made using equimolar solutions containing modified salicylaldehyde and 1,3-diamino-2-propanol in ethanol. In general, tetranuclear copper(II) compounds were made by combining stoichiometric amounts of H_3L, $Cu(ClO_4)_2.6H_2O$, and carboxylate linking mediator throughout MeOH (Scheme 3).

After double deprotonation, carboxylate bridging ligands (sodium oxalate, sodium malonate, sodium succinate, and terephthalic acid) coordinate as μ-bridging ligands. Our suggested general formula agrees with the elemental analyses of the H_3L and complexes **1–4**. These prepared compounds successfully recovered with good yields and were examined using various spectrophotometric methods. Attempts to obtain X-ray-grade crystals of these complexes were unsuccessful. In CH_3OH, estimated molar conductance parameters were obtained to be in the range of 25–35 Ω^{-1} cm^{-1} M^{-1} [31]. Figure S1 (Supplementary Information) shows the ESI-Mass of complexes **1–4**.

3.1. Powder X-ray diffraction

The molecular structures based on quantum chemical calculations (DFT) are given in Figure 1. The powder X-ray diffraction (XRD) morphologies from these compounds were carried out from the 2θ region = 0-90° to get the crystallinity of the compounds, as shown in Figure S2 (Supplementary Information). The most significant diffraction peaks are reported in Table 1. All complexes in their XRD pattern show a strong peak of ~25°, indicating that complexes **1–4** are crystalline and fine nanoparticles [32, 33]. The diffraction pattern of **3** and **4** with low angles with significant reflections at 14.19, 16.11, 26.69, and 28.11° and 17.30, 25.13, and 27.76°, respectively, indicate a higher crystallinity for these complexes to **1** and **2**.

3.2. Quantum chemistry

Using GAUSSIAN 09 application was used to conduct theoretical investigations (quantum chemical calculations) on the electronic structures of complexes **1–4** so terms of explaining its theorized geometric properties in the gaseous form [27, 28, 29]. Table S1 (Supplementary Information) contains the determined bond variables. This B3LYP basis set optimised the complex geometry (Figure 1). Figure S3 (Supplementary Information) displays contour plots of highly occupied molecular orbitals (HOMO) and lowest occupied molecular orbitals (LUMO), as well as the energy gap ΔE_g (HOMO-LUMO) [34]. The HOMO essentially acts as an electron donor and the LUMO as the electron acceptor [35]. Table 2 shows the predicted transition energy that was calculated. This ΔE_g value reflects upon its catalytic activity [36, 37]. The ΔE_g for **4** is the lowest, reflecting a relationship with SOD activity and could be regarded as an active centre for SOD mimics [36, 37, 38].

The graphical representations of the Mulliken spin densities for **1–4** are shown in Figure S4 (Supplementary Information). The delocalization of the single unpaired electron around the copper centres relates to $d^{22}_{x\text{-}y}$ with a less contribution d^2_z and donor atoms of complexes.

The energy gap (ΔE_g) of the present complexes (**1–4**) is observed to have the following order: **3** > **1** > **2** > **4**. Several global reactivity parameters are predicted using energy gap (ΔE_g), $E_{HOMO,}$ and E_{LUMO} values, which also describe the internal charge transport, stabilization, and reactivity of the molecules [38, 39] (Table 2). In HOMO and LUMO, three upper and three lower orbitals show distinct localization in all complexes, showing intramolecular electron charge transfer inside the molecule. The ΔE_g value is generally inversely proportional to the molecule's reactivity and softness and corresponds to its stability and hardness. Furthermore, modest energy gap numbers showed easy charge

Table 1. Data from X-ray diffraction of the complexes **1–4**.

Observed 2θ	Calculated 2θ	d spacing	h	K	l	Δ 2θ
Complex 1						
22.79	22.76	3.903	4	1	0	0.03
27.91	27.87	3.198	4	1	1	0.04
31.80	31.78	2.813	5	3	0	0.02
Complex 2						
17.41	17.39	5.095	1	1	2	0.02
21.99	21.98	4.00	0	1	4	0.01
28.94	28.93	3.083	-2	2	1	0.01
36.06	36.01	2.492	1	2	5	0.05
Complex 3						
14.19	14.17	6.244	-1	1	1	0.02
16.11	16.08	5.506	3	0	1	0.03
26.62	26.60	3.347	0	2	1	0.02
28.11	28.09	3.174	0	2	4	0.02
Complex 4						
17.30	17.28	5.128	0	0	4	0.02
25.13	25.10	3.551	-1	1	5	0.03
27.76	27.74	3.213	1	1	5	0.02

Table 2. Global reactivity descriptors for copper(II) complexes in eV.

Molecular properties	Mathematical description	1	2	3	4
E_{HOMO}	Energy of HOMO	-7.294	-6.715	-7.140	-6.947
E_{LUMO}	Energy of LUMO	6.639	-6.236	-5.176	-6.808
Energy gap	$\Delta E_g = E_{HOMO} - E_{LUMO}$	0.655	0.479	1.964	0.139
Ionization potential (IP)	$IP = -E_{HOMO}$	7.294	6.715	7.140	6.947
Electron Affinity (EA)	$EA = -E_{LUMO}$	6.939	6.236	5.176	6.808
Electronegativity (χ)	$(\chi) = -½ (E_{Homo} + E_{Lumo})$	7.116	6.475	6.158	6.878
Chemical Potential (μ)	$\mu = ½ (E_{Homo} + E_{Lumo})$	-7.116	-6.475	-6.158	-6.878
Global Hardness	$(\eta) = - ½ (E_{Homo} - E_{Lumo})$	0.327	0.240	0.982	0.069
Softness (S)	$(S) = 1/2\eta$	1.526	2.083	0.510	7.194
Electrophilicity index (ω)	$\omega = \mu^2/2\eta$	77.427	87.345	20.431	340.337

transfer inside the molecule, which might boost the complex biological processes even more.

Each copper(II) ion in complexes (**1–4**) is four coordinated. The copper centres are coordinated by phenolic oxygen, azo nitrogen, alkoxy oxygen, and carboxylic oxygen atoms. Cu–N/Cu–O bond lengths anticipated for such complexes appear close to those described in four coordinate copper complexes based on X-ray data [40]. The geometry index number with each Cu ion was distinct. Yet, a review among those index values reveals that Cu1, Cu3, and Cu4 (τ_4 = 0.850-0.705) centres are approximately tetrahedral, whereas Cu2 (τ_4 = 0.690-0.463) centre has neither tetrahedral nor square planar [41] (Table 3).

Table 3. Geometry Index (τ_4) variables for copper(II) complexes.

Complex	Geometry Index (τ4)			
	Cu1	Cu2	Cu3	Cu4
1	0.723	0.483	0.741	0.760
2	0.850	0.690	0.846	0.816
3	0.705	0.513	0.789	0.829
4	0.743	0.463	0.829	0.753

3.3. NMR spectra

The mutual utilization of experimental and Gaussian computational tools provides exciting information about the structures of molecules. Figures S5 and S6 (Supplementary Information) show the results of the ^{1}H and ^{13}C NMR experiments. The ^{1}H NMR spectrum in DMSO has peaks at δ = 13.571 and 13.586 ppm due to phenolic proton (s, 2H, OH), while the peak at δ = 8.524 ppm has two azo protons (s, 2H, CH = N). The peak has a chemical shift of 3.807 due to methoxy proton (s, 3H, OCH_3). The peaks having medium-range chemical shifts (6.888–7.571 ppm) are due to the aromatic protons (s, 5H, ArH). The peak corresponding to the alkoxy group of H_3L appears to be δ = 4.026 (s, 14, C–OH). At the lowest δ (s/d, 3.767-3.407), the peaks are due to methylene protons attached to nitrogen atoms (s, 4H, N–CH_2).^{13}C NMR spectrum reveals peaks at δ = 160.51 and 166.42 ppm because the benzene ring's C-atoms are linked to OH (s, 2C, Ar-ring). Two peaks at 131.01 and 132.49 ppm are attributable to the group's azo (HC = N) of H_3L (m, 2C CH = N). The peaks at 62.97 and 69.54 ppm are due to methoxy (s, 1C, OCH_3) and CH_2 moiety of methylene (s, 2C, CH_2–N) carbon atoms. The peaks observed in the range of δ = 119.17–122.03 ppm are due to carbon atoms of the benzene

Table 4. FTIR spectral assignments (cm^{-1}) for Schiff base ligand H_3L and complexes **1–4**.

Compounds	ν(C=N)	ν(C–H)	ν(Cu–O)	ν(Cu–N)
H_3L	1649	3058	-	-
1	1600	3089	460	437
2	1569	-	464	447
3	1596	1550	622	419
4	1668	1550	568	461

Table 5. Electronic spectral values in CH_3OH solvent.

Compound	λmax (nm)		
	π→π*/n→π*	CT band	*d-d* band
H_3L	350	-	-
1	325	390	630
2	326	391	631
3	325	390	631
4	327	392	629

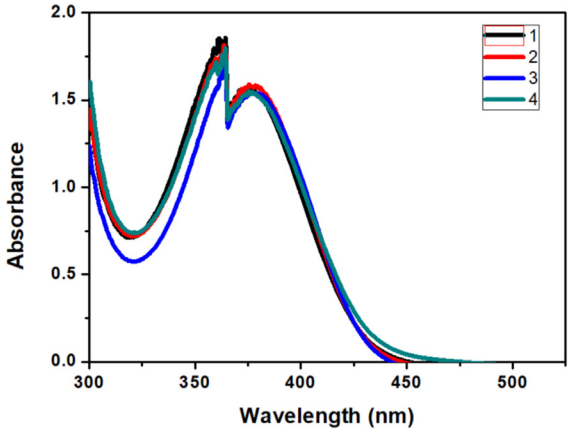

Figure 2. LMCT spectra of complexes **1–4** in 1 × 10^{-3} M DMSO solution.

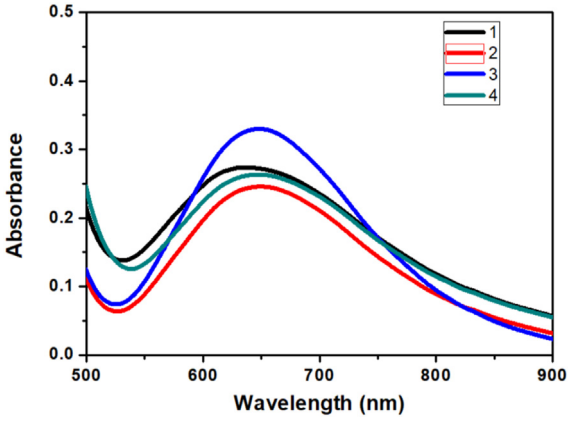

Figure 3. Absorption spectra of complexes **1–4** showing d-d transitions in 1 × 10^{-3} M DMSO solution.

ring (s, 5C, Ar-ring). Theoretically calculated ^{1}H NMR and ^{13}C NMR spectral peak positions compare well with experimental peak positions (Table S2) (Supplementary Information). The theoretical spectral peaks showed a good correlation with experimental values.

3.4. FTIR spectral studies

The infrared spectral data of the ligand H_3L and complexes **1–4** are given in Table 4, with their tentative assignments. Complexes demonstrated ν(C=N) stretching band, a feature of Schiff base ligands at 1668-1569 cm^{-1}, which shifted to the lower frequency side by ~10–26 cm^{-1} [42, 43, 44]. Characteristic bands of the aromatic ν(C–H) vibrations appear at 3057-3173 cm^{-1}. The coordinated azomethine nitrogen atoms in complexes confirmed the appearance of new bands within the range 622-460 cm^{-1} ascribed to ν(Cu–N). In all complexes, the –OH (hydroxyl) proton is removed in the basic medium, and the oxygen atom is

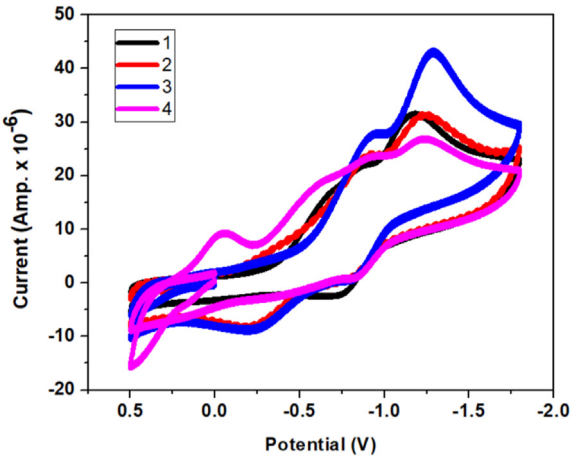

Figure 4. Cyclic voltammograms of Complexes **1–4** in DMSO solvent at a scan rate of 300 mV s^{-1} and a temperature of 25 °C on an Ag/AgCl electrode.

coordinated to copper. With the addition of such band to the lineup, ~ 461-419 cm^{-1} and 460-622 cm^{-1} in spectra complexes are ascribed to ν(Cu–N) and ν(Cu–O), respectively [44]. The optimized geometries of H_3L and complexes (**1–4**) were used to calculate FTIR absorption frequencies at the same B3LYP/6-311G level to explore their stability. The DFT calculations correlate with these assignments and exhibit the same trend as found with experimentally observed peaks for ν(C=N). From theoretical calculated peaks ν(C=N) for H_3L and complexes observed at 1693, 1685, 1690, 1680, and 1653 cm-1, respectively. These values are compared with experimentally observed peaks (Table 4).

3.5. UV-visible analysis

H_3L compounds and complexes **1–4** had their electronic spectra reported by 1.0 × 10^{-3} DMSO solution, and the λ_{max} (nm) are summarized in Table 5. UV-visible absorption spectra are shown in Figures 2 and 3. For comparison, the electronic spectrum H_3L is also measured. H_3L and its compounds have bands in the 300–350 nm range that match the π→π*/n→π* transitions. The LMCT band may be seen from the 391 ± 1 nm range (Figure 2). The copper(II) ions are in the planner setting because all complexes have d-d transition bands in the region 630 ± 1 nm (Figure 3) [45, 46]. TD-DFT calculations were carried out with B3LYP/LANL2DZ with implicit solvation to aid in the electronic spectra of complexes. When comparing the theoretical absorption peaks of four coordinated double bridged complexes (**1–4**) to the experimentally observed, the DFT predicts the only two peaks at ~ 325 and ~700 nm. These absorption peaks, which are 325 and 630 nm, are in accord with experimental findings. The higher energy bands are owing to the π→π* transition in the ligand backbone, and lower energy bands are due to the *d-d* transition.

3.6. Electrochemistry of complexes

In an N2 environment, the cyclic voltammogram of complexes 1–4 in DMSO 1 × 10-3 M was obtained at room temperature with 0.1M TBAP like a supporting electrolyte (Figure 4). All complexes show quasi reversible cathodic reduction peaks, and redox data are given in Table 6. The two reduction processes vs the Ag/AgCl reference, as demonstrated by the DPV studies, both involve roughly equivalent electrons (Figure 5). The formal potentials of two reduction potentials vary by over 180 Mv, according to DPV [47, 48]. Reduction process for the Cu(II)/Cu(I) couple (a process I) comes out ~ -0.05 V in relation to it Ag/AgCl electrode. These reduction waves are quasi reversible. The observed additional peaks in the DPV may be due to the reduction of the ligand moieties (Figure 5). The reduction at more negative potential (process II)

Table 6. Electrochemical parameters for complexes **1–4**.

Complex	E_{pc1}(V)	E_{pc2}(V)	E_{pc1}(V)	E_{pa2}(V)	DE_{c1}(V)	DE_{c2}(V)	ΔD_{pc}(V)	$E^1_{½}$(V)	$E^1_{½}$(V)	$\Delta E_{½}$(V)	K_{con}
1	-0.864	-1.184	-0.736	-1.12	-0.683	-0.923	-0.240	-0.80	-1.152	0.352	5.887×10^8
2	-0.902	-1.238	-0.224	-0.821	-0.693	-0.966	-0.273	-0.563	-1.029	0.466	7.749×10^8
3	-0.926	-1.291	-0.221	-0.818	-0.715	-1.008	-0.190	-0.579	-1.054	0.475	8.105×10^8
4	-0.923	-1.238	-0.331	-0.838	-0.704	-0.998	-0.294	-0.627	-1.038	0.411	6.881×10^8

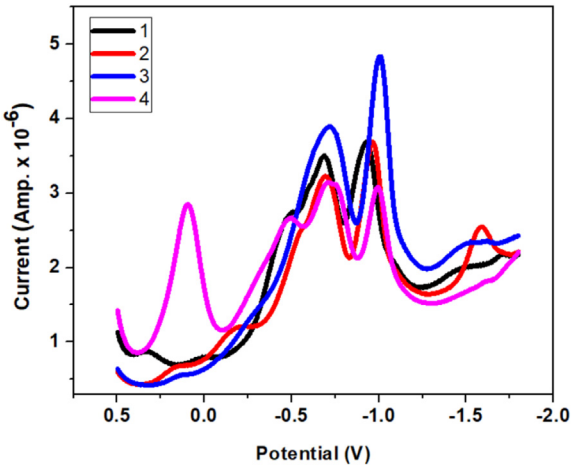

Figure 5. Differential pulse voltammograms of complexes **1–4** at 25 °C using a scan rate of 20 mVs^{-1} in DMSO.

corresponds to CuIICuICuICuI redox couples. As indicated in Eqs. (1) and (2), these reduction processes (I and II) are provisionally attributed to one-electron processes [49, 50].

$$Cu^{II}Cu^{II} \longrightarrow Cu^{II}Cu^{I} \quad (1)$$

$$Cu^{II}Cu^{I} \longrightarrow Cu^{I}Cu^{I} \quad (2)$$

Complexes **1–4** have a reduction potential similar to those described in the literature. For **3**, an significant $\Delta E_{1/2} = 0.475$ V result is calculated, indicating strong metal-metal interactions and combination to strong spin-spin interactions [50]. The conproportionation constant (K_{con}), which shows the stability of mixed valent complexes ($Cu^{II}Cu^{I}$), was also evaluated for the following Eq. (3).

$$Cu^{II}\ Cu^{II} + Cu^{I}\ Cu^{I} \overset{K_{con}}{\rightleftharpoons} 2Cu^{II}\ Cu^{I} \quad (3)$$

Due to the enormous K_{con} values, it is clear that adding a second electron is difficult, and hence the $Cu^{II}Cu^{I}$ mixed-valence species is conproportionation stable. Multinuclear complexes are more prone to this phenomenon. The K_{con} of **3** was highest than other complexes, which shows that complex **3** is the most stable.

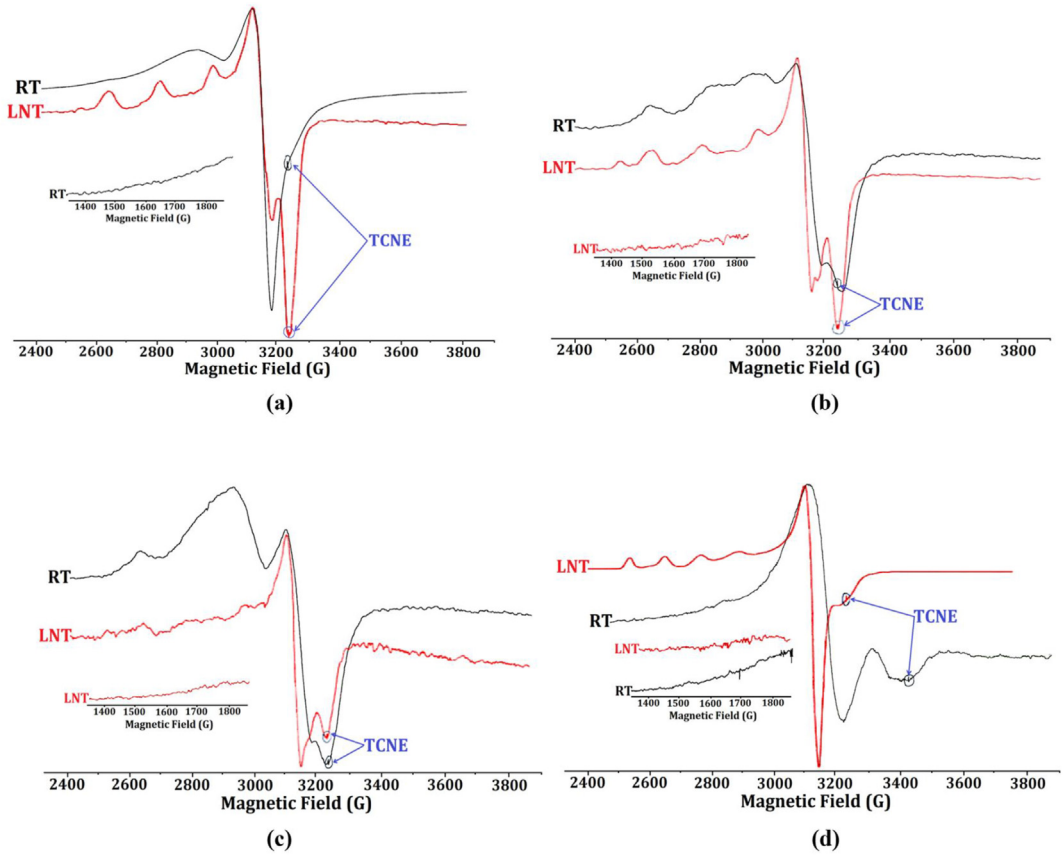

Figure 6. Epr spectra in the polycrystalline state (RT) and DMSO solution at LNT for (a) complex 1 (b) complex 2 (c) complex 3 (d) complex 4.

Table 7. Epr values of copper(II) complexes **1–4**.

Compounds	RT					LNT		
	$g_{\parallel}$	$g_{\perp}$	D(cm^{-1})	E (cm^{-1})	G	$g_{\parallel}$	$g_{\perp}$	$A_{\parallel}$(G)
1	2.189	2.053	0.062	0.002	3.734	2.209	2.060	170
2	2.194	2.051	0.058	0.002	3.996	2.246, 2.215	2.071	170, 170
3	2.205	2.054	0.055	0.002	3.920	2.205	2.071	160
4	2.223	2.074	0.056	0.002	3.078	2.267, 2.220	2.071	115, 120

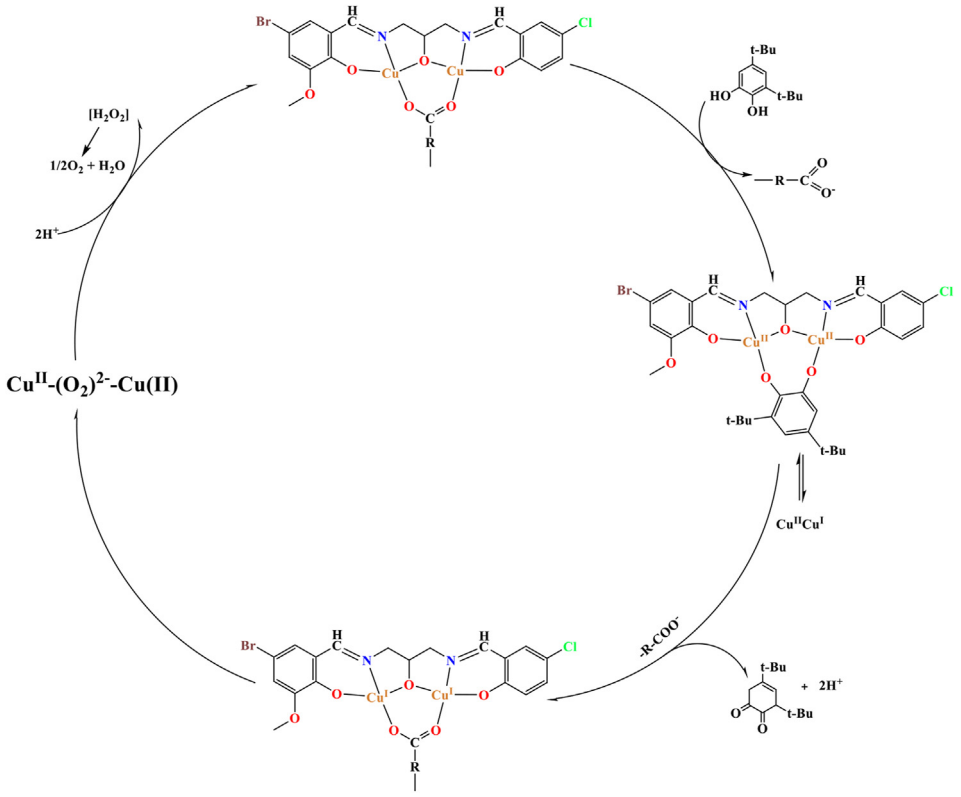

Scheme 4. The mechanism for the 3,5-dtbc oxidation is catalyzed by copper(II) complexes.

3.7. Epr studies of copper(II) tetranuclear complexes

At ambient temperature in the polycrystalline form and liquid nitrogen temperature in 1.0×10^{-3} M DMSO, Epr spectra for four tetranuclear compounds are generated. The room temperature polycrystalline spectra are broad, and a broad signal appears in each spectrum. Figure 6 shows the overall Epr spectra of complexes **1–4** and the computed Epr values in Table 7.

In complex **4**, at high field, one additional broad signal appears. Similar spectral features have already been observed for other copper(II) tetranuclear complexes [51]. These Epr spectra are satisfactorily analyzed owing to an S = 2 species with $g_{\parallel}$ $g_{\perp}$ D and E. The inner aspects of these Epr spectra may be attributed to the tetramer's quintet state (S = 2), while the outer resonance can be attributed to the tetramer's triplet state (S = 1) [51]. Using such hypotheses, the D numbers for zero-field splitting in tetramer complexes were estimated and shown in Table 7. The zero-field energy E was also evaluated and collected in Table 7. The Spin-spin exchange parameter (G) is less than 4, showing spin-spin exchange interactions in all complexes.

Epr spectra at LNT in DMSO frozen solution were already obtained and analyzed at low temperatures. The Epr spectra for **1** and **3** arise from the mononuclear copper(II) complex. Such spectral features suggest that the polynuclear complex is dissociated into mononuclear species after dissolving in DMSO [52, 53, 54]. The spectral pattern and Epr parameters of both complexes are typical of an axial copper(II) complex of a Schiff base [55, 56]; on the other hand, the spectra' of the remaining two complexes (**2** and **4**) show septet feature in $g_{\parallel}$ the region. Such features are due to the presence of more than one species due to intradimer spin-exchange interactions indicative of undissociated complex in solution. Analogous spectrum characteristics were described in polynuclear Cu(II) complexes [57].

3.8. Kinetics for 3, 5-di-tert-butyl catechol activity

All synthesized complexes (**1–4**) were created as both structure and function prototypes of catechol oxidase enzyme; hence determining catecholase-like performance becomes critical. All complexes (**1–4**) show moderate catalytic activity. Scheme 4 depicts the hypothesized catalytic activity mechanism. The two-electron oxidation of 3,5-dtbc to quinone was evaluated by the transmission of pair of an electron from the Cu(II)–Cu(II) active site leading to its lowering into Cu(I)–Cu(I). So when quinone becomes disorganized, it interacts with oxygen molecules (O_2) in the precursor solution, causing the Cu(I)–Cu(I) core to reoxidize, releasing a water molecule and recovering a catalyst [20, 21, 22, 23]. The reaction product 3,5-tertbutyl-o-quinone (3,5-dtbq) is appreciable stable and shows a strong absorption at ~ 400 nm due to quinone formation (C=O). A rise in quinone band increasing duration was seen in all **1–4** complexes, as illustrated in Figure 7. A technique using initial rates was

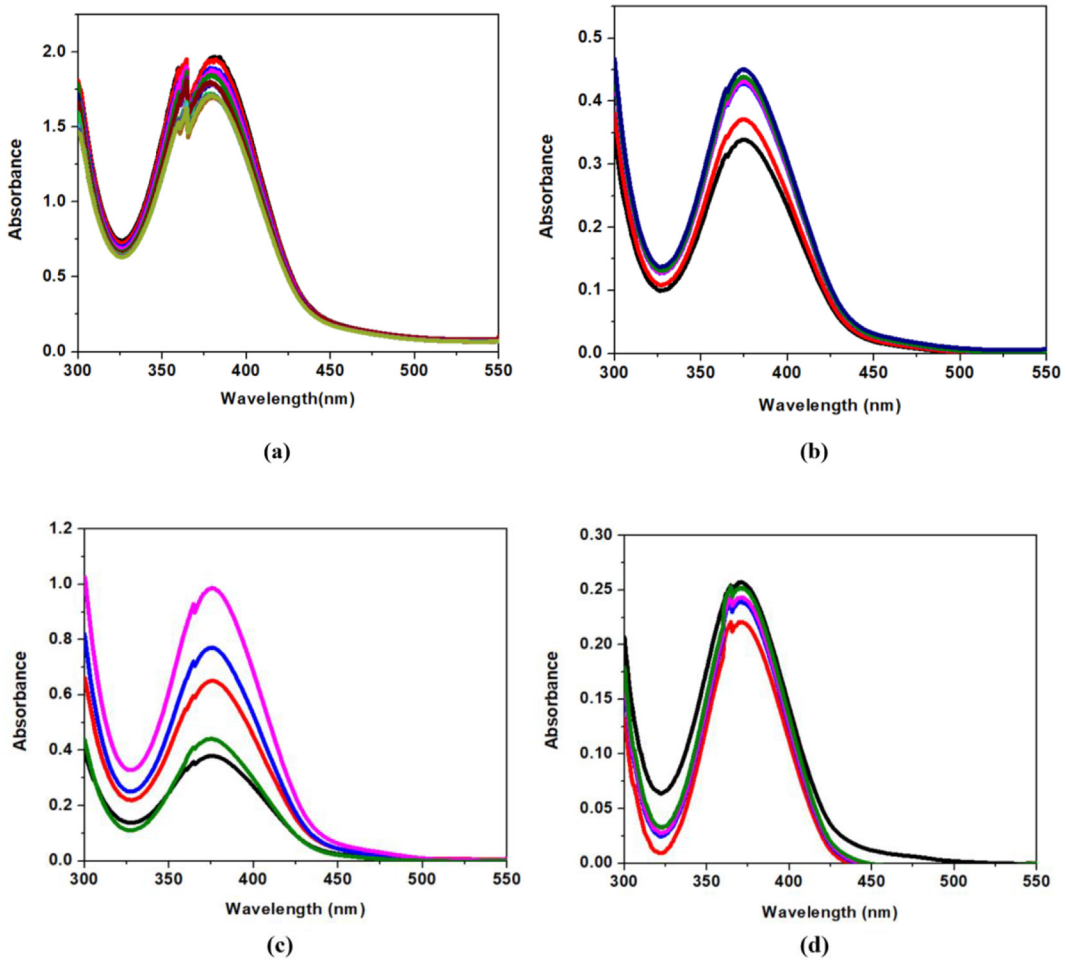

Figure 7. Time-dependent growth of 3,5-dtbc catalyzed through (a) complex **1** (b) complex **2** (c) complex **3** and (d) complex **4**.

Table 8. Kinetic data of dtbc oxidation reaction catalyzed by binuclear complexes **1–4.**

Complex	V_{max} (min^{-1})	K_m (M)	K_{ass} (M^{-1})	k_{cat} (h^{-1})	k_{cat}/K_m (M h^{-1})
1	0.018	42	238(2.38×10^2)	0.125 (7.50 min^{-1})	2.976×10^{-4}
2	0.019	24	417(4.17×10^2)	0.129 (7.74 min^{-1})	5.375×10^{-4}
3	0.014	25	400(4.0×10^2)	0.099 (5.94 min^{-1})	3.960×10^{-4}
4	0.020	28	357(3.57×10^2)	0.125 (7.50 min^{-1})	4.400×10^{-4}

used to study its kinematics of 3,5-dtbc oxidation by complexes **1–4**, which involved measuring its growth mainly in a typical 3,5-dtbq band around 400 nm at a time-dependent. The slope of the first-order kinetics fitting data at the beginning of the reaction, whenever the backward response is presumed inconsequential, can be used to derive the starting rate [V_0] for each substrate concentration. All acquired results were analyzed using Michaelis-Menten enzymatic kinetics technique [21]. The enzymatic kinetic parameters estimated from the Lineweaver-Burk plots are shown in Figure S7 (Supplementary Information), and calculated parameters are summarized in Table 8. Scheme 4 depicts the suggested process of 3,5-dtbc oxidation catalyzed with complexes.

The medium behaviour of complexes **1–4** is indicated by increased K_m and small k_{cat} readings. Complex **2** ($k_{cat} = 0.129\ h^{-1}$) is a better catalyst model than the remaining complexes when compared to reported catalytic variable (K_m and k_{cat}) data for those other metal complexes having comparable enzymatic catalytic properties [58, 59]. A coordination ring surrounding metal(II) ions and metal-metal spacing are two main variables that govern the catalytic performance of metal complexes [11, 60, 61, 62]. The variation in exercise among complexes **1–4** might be due to the second component.

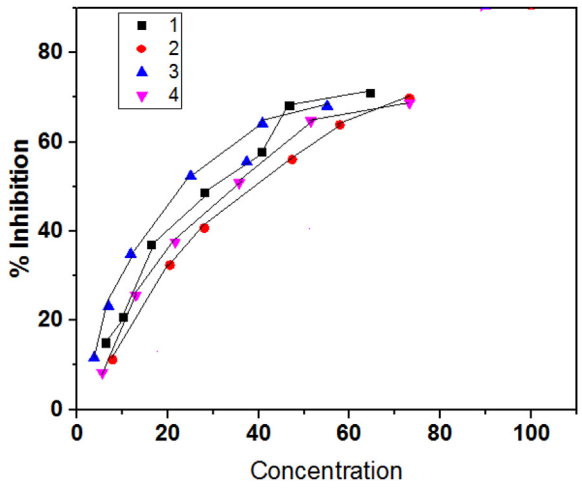

Figure 8. A plot of % inhibition of NBT reduction *vs* concentration of complexes **1–4**.

Table 9. SOD activity data (IC_{50}, K_{McCF}, and SOD activity) of copper(II) complexes.

Compound	IC_{50} (μM)	SODactivity (μM^{-1})	$k_{cat} \times 10^4$ $M^{-1}s^{-1}$	Reference
V_C	852	1.17	0.39	[66]
$[Cu_2\mu(SCN)_2L^1{}_2]$	24	41.66	13.84	[65]
$[Cu(L^2)(NO_3)(\mu\text{-}2\text{-}aminopyrazine)Cu(L^2)(NO_3)_2].2H_2O$	15	66.67	22.17	[67]
$[(L^3)Cu(\mu\text{-}CH_3COO)_2Cu(L^3)]$	35	28.57	9.50	[68]
$[(L^3)Cu(\mu\text{-}NO_3)_2Cu(L^3)]$	26	38.46	12.79	[68]
$[Cu_2(Z\text{-}(2\text{-pyridyl})benzimidazole)_2(L^4{}_2)]ClO_4$	17	58.82	19.57	[49]
1	31	32.26	10.73	This work
2	40	25.00	8.31	This work
3	23	43.48	14.46	This work
4	35	40	9.50	This work

L^1 =(Z)-N'-(phenyl(pyridin-2-yl)methylene)acetohydrazide, L^2 = N'-[(E)-phenyl (pyridine-2-yl)methylidene]benzohydrazide, L^3 = L = N'- [phenyl(pyridin-2-yl) methylidene]benzohydrazone), L^4 = N'-[(E)-phenyl (pyridine-2-yl)methylidene]furon-2- carbo-hydrazide.

3.9. SOD activity

All four complexes exhibit catalytic activity toward the dismutation of $O_2^{\cdot-}$ at physiological pH, $O_2^{\cdot-}$ enzymatically supplied from the alkaline DMSO and SOD activities were evaluated by NBT assays [25, 63, 64], following the reduction of NBT to MF^+ at ~ 500 nm kinetically. Figure 8 depicts the Superoxide plot. The evaluated IC_{50} values of present complexes remain in the range of 23–40 μM. The structural variation among the existing complexes might explain the slight variances in activity statistics. A observed trend in Superoxide dismutase for all these compounds is **3** > **1** > **4** > **2**. These values are in the same order of magnitude as the SOD mimics (IC_{50} = 15–852 μm) reported in the literature [65, 66, 67]. The above compounds' SOD activity was also measured and compared to that of similar SOD mimics (Table 9).

Another possible reason may be the very high binding constants between the dicarboxylate ions and dinuclear complexes. The above compound catalytic rate constant (k_{cat}) was determined [49, 66, 67, 68]. Similar to other compounds mentioned in the literature, its topology surrounding a copper(II) centre stays deformed square planar, indicating acceptable SOD activity [65, 66, 67, 68]. Scheme 5 depicts the hypothesized process for a typical complex catalytic activity.

3.10. Structure-activity relationship analysis

Calculated SOD value for complexes (**1–4**) demonstrates how SOD activity is significantly higher with catecholase efficiency for such complexes. The $Cu^{II}NO_3$ structural motif seems to be to blame for this discovery. The active sites of Cu–Zn SOD are almost identical to the binding sites of catechol oxidase. Furthermore, the catecholase activity demonstrated by Cu–N functional component could be harmed by the Cu–O functional component. So, the SOD and catecholase activity. Electrochemical experiments and quantum chemistry simulations also provided

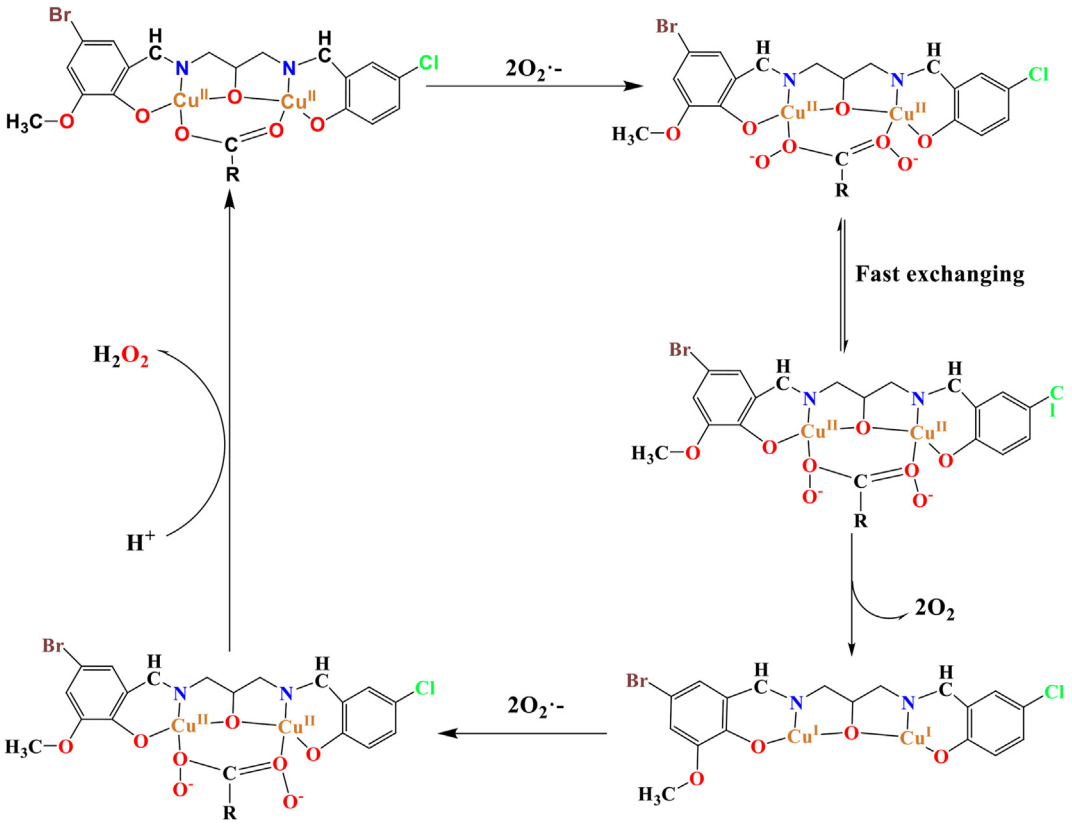

Scheme 5. Catalytic mechanism of $O_2^{\cdot-}$ dismutation through the complex.

insight into the structural-activity connection for such $CuNO_3$ analogues, complexes **1–4**. The results show that such complexes have electron-accepting capacities and coordination situations that have been influenced by the complexes' connecting groups. The action of SOD and catecholase is affected by such bridged groups. SOD development is linked to the transformation of $O_2^{\cdot-}$ O_2, during which action, the copper(II) centre obtains extra electrons from $O_2^{\cdot-}$ [69]. As a result, it is therefore believed that indeed more excellent the complex's electron-accepting capacity, the more advantageous the electron transfer from $O_2^{\cdot-}$ copper(II) will be; therefore, SOD activity will increase. Similarly, the catecholase function involves a method of transferring electrons that are obtained via copper (II) [70]. As a result, it is therefore envisaged that enhancing a metal complex's acceptors potential will increase catecholase efficiency.

The catalytic performance of a compound is related to its electrochemical features. The quasi reversible reduction waves are assigned to Cu^{II}/Cu^{I} pairs. E results indicate its electron-accepting powers are already in the **4** > **3** > **2** > **1** range, which corresponds to the catecholase (k_{cat}) task variability trend. According to the mechanism of bioactivity information and electrolytic information, increasing the electron-accepting potential of complexes seems to have a significant impact on their mimetic behaviours.

Furthermore, quantum chemical calculations were carried out to show an additional analysis of the enzymatic activities of the complexes. Similarly, ΔE_g is an essential criterion for showing enzymatic biological activities [71, 72]. According to ΔE_g, the biological activity pattern is almost the same as that seen in SOD/catecholase activities. Considering the findings mentioned above, it is clear that the electron-accepting capacity of complexes plays an integral part in describing their bioactivity.

4. Conclusions

The tetranuclear copper(II) complexes were produced utilizing a tridentate Schiff base and μ-carboxylate bridging binder. Spectral, electrochemical, and catalytic studies have been conducted on these compounds. Epr spectral features can be assigned to quintet (S = 2) central part and outer resonance of triplet (S = 1) of the tetramer. To acquire molecule structures and investigate reactivity characteristics, quantum mechanical simulations have been used. The used ligand and its complexes are stable, less polarizable, and of hard nature from the values of reactivity parameters signifying the resistance toward deformation of the electron density of molecule under small perturbation. Furthermore, all catecholase and SOD activity data were assessed and compared to reported duplicates. According to with findings, present complex **3** now had maximum Scavenging activity.

Declarations

Author contribution statement

Abhay K. Patel, Neetu Patel: Performed the experiments; Analyzed and interpreted the data.

R. N. Patel, Rajendra N. Jadeja: Conceived and designed the experiments; Contributed reagents, materials, analysis tools; Wrote paper.

Funding statement

This research did not receive any specific grant from funding agencies in the public, commercial, or not-for-profit sectors.

Data availability statement

Data included in article/supplementary material/referenced in article.

Declaration of interests statement

The authors declare no conflict of interest.

Additional information

Supplementary content related to this article has been published online at https://doi.org/10.1016/j.heliyon.2022.e09373.

Acknowledgements

The authors are thankful to SAIF IIT Mumbai for ESR measurements, SAIF CDRI Lucknow for microanalysis, and SAIF IIT Ropar for ESI-Mass analysis.

References

[1] K.D. Karlin, Z. Tyeklar (Eds.), Bioinorganic Chemistry of Copper, Chapman & Hall, New York, 1993.
[2] B. Reinhammer, Copper Proteins and Copper Enzymes, vol. 3, CRC Press, Boca Raton, FL, 1984, pp. 1–35.
[3] T.G. Spiro, Copper Proteins, Wiley-Interscience, New York, 1981.
[4] H. Decker, R. Dillinger, F. Tuczek, How does tyrosinase work recent insights from model chemistry and structural biology, Angew. Chem. Int. Ed. 39 (2000) 1591–1595.
[5] C. Gerdemann, C. Eicken, B. Krebs, The crystal structure of catechol oxidase: new insight into the function of type-3 copper proteins, Acc. Chem. Res. 35 (2002) 183–191.
[6] P. Gentschev, M. Luken, N. Moller, A. Rompel, B. Krebs, Synthesis of a novel μ-acetate bridged dinuclear Cu(II) complex as a model compound for the active site of tyrosinase: crystal structure, magnetic properties and catecholase activity, Inorg. Chem. Commun. 4 (2001) 753–756.
[7] C. Eicken, B. Krebs, J.C. Sacchettini, Catechol oxidase - structure and activity, Curr. Opin. Struct. Biol. 9 (1999) 677–683.
[8] T. Klabunde, C. Eicken, J.C. Sacchettini, B. Krebs, The Crystal structure of a plant catechol oxidase containing a dicoppercenter, Nat. Struct. Biol. 5 (1998) 1084–1090.
[9] S. Mistri, A. Paul, A. Bhunia, R.K. Manne, M.K. Santra, H. Puschmann, S.C. Manna, A combined experimental and theoretical investigation on the Cu(II) sensing behavior of a piperazinyl moiety based ligand, and catecholase and biological activities of its Cu(II) complex in combination with pyridine 2,5-dicarboxylate, Polyhedron 104 (2016) 63–72.
[10] E. Monzani, L. Quinti, A. Perotti, L. Casella, M. Gulloti, L. Randaccio, S. Geremia, G. Nardin, P. Faleschini, G. Tabbi, Tyrosinase models. Synthesis, structure, catechol oxidase activity, and phenol monooxygenase activity of a dinuclear copper complex derived from a triamino pentabenzimidazole ligand, Inorg. Chem. 37 (1998) 553–562.
[11] C. Belle, C. Beguin, I. Gautier-Luneau, S. Hamman, C. Philouze, J.L. Pierre, F. Thomas, S. Torelli, E. Saint-Aman, M. Bonin, Dicopper(II) complexes of H-BPMP-Type ligands: pH-induced changes of redox, spectroscopic (19F NMR studies of fluorinated complexes), structural properties, and catecholase activities, Inorg. Chem. 41 (2002) 479–491.
[12] M. Tremolieres, J.G. Bieth, Isolation and characterization of the polyphenoloxidase from senescent leaves of black poplar, Phytochemistry 23 (1984) 501–505.
[13] S.C. Cheng, H.H. Wei, Structure, magnetic properties and catecholase activity study of oxo-bridged dinuclearcopper(II) complexes, Inorg. Chim. Acta. 340 (2002) 105–113.
[14] P.A. Vigato, S. Tamburini, D.E. Fenton, The activation of small molecules by dinuclear complexes of copper and other metals, Coord. Chem. Rev. 106 (1990) 25–170.
[15] R.E.H.M.B. Osorio, R.A. Peralta, A.J. Bortoluzzi, V.R. de Almeida, B. Szpoganicz, F.L. Fischer, H. Terenzi, A.S. Mangrich, K.M. Mantovani, D.E.C. Ferreira, W.R. Rocha, W. Haase, Z. Tomkowicz, A. dos Anjos, A. Neves, Synthesis, magnetostructural correlation, and catalytic promiscuity of unsymmetric DinuclearCopper(II) complexes: models for catechol oxidases and hydrolases, Inorg. Chem. 51 (2012) 1569–1589.
[16] J.S. Miller, M. Drillon, Magnetism: Molecules to Materials, Wiley VCH, Weinheim, 2002.
[17] A.L. Barra, A. Caneschi, A. Cornia, F. Fabrizi de Biani, D. Gatteschi, C. Sangregorio, R. Sessoli, L. Sorace, Single-molecule magnet behavior of a tetranuclear iron(III) complex. The origin of slow magnetic relaxation in iron(III) clusters, J. Am. Chem. Soc. 121 (1999) 5302–5310.
[18] C. Lopez, R. Costa, F. Illas, C.de. Graaf, M.M. Turnbull, C.P. Landee, E. Espinosa, I. Matae, E. Molinse, Magneto-structural correlations in binuclear copper(ii) compounds bridged by a ferrocenecarboxylato(−1) and an hydroxo- or methoxo-ligands, Dalton Trans. (2005) 2322–2330.
[19] C.J. Boxwell, R. Bhalla, L. Cronin, S.S. Turner, P.H. Walton, Self-assembly preparation, structure and magnetic studies of a novel dinuclearcopper(II) complex: [Cu2(μ-OH)(μ-OAc)(μ-L)][BF4]2 [L = bis-1,3-(*cis,cis*-1,3,5-triaminocyclohexane) xylylidiene], J. Chem. Soc. Dalton Trans. (1998) 2449–2450.

[20] S.K. Day, A. Mukherjee, Catechol oxidase and phenoxazinone synthase: biomimetic functional models and mechanistic studies, Coord. Chem. Rev. 310 (2016) 80–115.
[21] C.S. Foote, J.S. Valentine, A. Greenberg, J.F. Liebman, Active oxygen in chemistry, Struct. Energ. React. Chem. Ser. 2 (1995) 1995.
[22] K.D. Karlin, M.S. Nasir, B.I. Cohen, R.W. Cruse, S. Kaderli, A.D. Zuberbiihle, Reversible dioxygen binding and aromatic hydroxylation in O2-reactions with substituted xylyl dinuclear copper(I) complexes: syntheses and low-temperature kinetic/thermodynamic and spectroscopic investigations of a copper monooxygenase model system, J. Am. Chem. Soc. 116 (1994) 1324–1336.
[23] K.D. Karlin, N. Wei, B. Jug, S. Kaderli, P. Niklausf, A.D. Zuberbiihler, Kinetics and thermodynamics of formation of copper-dioxygen adducts: oxygenation of mononuclear copper(I) complexes containing tripodal tetradentate ligands, J. Am. Chem. Soc. 115 (1993) 9506–9514.
[24] J. Vančo, O. Švajlenová, E. Račanská, J. Muselík, J. Valentová, Antiradical activity of different copper(II) Schiff base complexes and their effect on alloxan-induced diabetes, J. Trace Elem. Med. Biol. 18 (2004) 155–161.
[25] R.G. Bhirud, T.S. Shrivastava, Superoxide dismutase activity of Cu(II)2(aspirinate)4 and its adducts with nitrogen and oxygen donors, Inorg. Chim. Acta. 173 (1990) 121–125.
[26] R. Konecny, J. Li, C.L. Fisher, V. Dillet, D. Bashford, L. NoodlemanL, CuZn superoxide dismutase geometry optimization, energetics, and redox potential calculations by density functional and electrostatic methods, Inorg. Chem. 38 (1999) 940–950.
[27] M.J. Frisch, G.W. Trucks, H.B. Schlegel, G.E. Scuseria, M.A. Robb, J.R. Cheeseman, G. Scalmani, V. Barone, B. Mennucci, G.A. Petersson, H. Nakatsuji, M. Caricato, X. Li, H.P. Hratchian, A.F. Izmaylov, J. Bloino, G. Zheng, J.L. Sonnenberg, M. Hada, M. Ehara, K. Toyota, R. Fukuda, J. Hasegawa, M. Ishida, T. Nakajima, Y. Honda, O. Kitao, H. Nakai, T. Vreven, J.A. Montgomery Jr., J.E. Peralta, F. Ogliaro, M. Bearpark, J.J. Heyd, E. Brothers, K.N. Kudin, V.N. Staroverov, R. Kobayashi, J. Normand, K. Raghavachari, A. Rendell, J.C. Burant, S.S. Iyengar, J. Tomasi, M. Cossi, N. Rega, J.M. Millam, M. Klene, J.E. Knox, J.B. Cross, V. Bakken, C. Adamo, J. Jaramillo, R. Gomperts, R.E. Stratmann, O. Yazyev, A.J. Austin, R. Cammi, C. Pomelli, J.W. Ochterski, R.L. Martin, K. Morokuma, V.G. Zakrzewski, G.A. Voth, P. Salvador, J.J. Dannenberg, S. Dapprich, A.D. Daniels, O. Farkas, J.B. Foresman, J.V. Ortiz, J. Cioslowski, D.J. Fox, Gaussian 09, Revision D.01, Gaussian Inc., Wallingford CT, 2009.
[28] P.J. Hay, W.R. Wadt, Ab initio effective core potentials for molecular calculations. Potentials for the transition metal atoms Sc to Hg, J. Chem. Phys. 82 (1985) 299–310.
[29] Gauss View 5.0.9, Gaussian Inc., Wallingford, CT, U.S.A., 2009.
[30] A.E. Reed, R.B. Weinstock, F. Weinhold, Natural population analysis, J. Phys. Chem. 83 (1985) 735–746.
[31] W.J. Geary, The use of conductivity measurements in organic solvents for the characterization of coordination compounds, Coord. Chem. Rev. 7 (1971) 81–122.
[32] M.S. Nair, R.S. Joseyphus, Synthesis and characterization of Co(II), Ni(II), Cu(II) and Zn(II) complexes of tridentate Schiff base derived from vanillin and DL-alpha-aminobutyric acid, Spectrochim. Acta 70 (2008) 749–753.
[33] S.A. Sallam, Binuclear copper(II), nickel(II) and cobalt(II) complexes with N_2O_2 chromophores of glycylglycine schiff-bases of acetylacetone, benzoylacetone and thenoyltrifluoroacetone, Transit. Met. Chem. 31 (2006) 46–55.
[34] D. Shobaa, S. Periandy, M. Karabacak, S. Ramalingam, Vibrational spectroscopy (FT-IR and FT-Raman) investigation, and hybrid computational (HF and DFT) analysis on the structure of 2,3-naphthalenediol, Spectrochim. Acta 83 (2011) 540–552.
[35] K. Fukui, Role of frontier orbitals in chemical reactions, Science 218 (1982) 747–754.
[36] Q. Wang, D. Chen, X. Liu, L. Zhang, Theoretical mechanisms of the superoxide radical anion catalyzed by the nickel superoxide dismutase, Comput. Theor. Chem. 966 (2011) 357–363.
[37] Xtao-Li Cui, Da-Sen Ren, Song-Tao Wo, Jie Shen, Xi-Liang Yang, Zhuang-Jian Zhang, Two photoelectrochemical processes for TiO2 electrode under UV illumination, Chin, J. Chem. 21 (2003) 1001–1004.
[38] R. Jawari, M. Haussian, M. Khalid, M.U. Khan, M.N. Tahir, M.M. Naseer, A.A.C. Barga, Z. Shafiq, Synthesis, crystal structure analysis, spectral characterization and nonlinear optical exploration of potent thiosemicarbazones based compounds: a DFT refine experimental study, Inorg. Chim. Acta. 486 (2019) 162–171.
[39] T. Koopmans, Über die Zuordnung von Wellenfunktionen und Eigenwertenzu den Einzelnen Elektronen Eines Atoms, Physica 1 (1934) 104–113.
[40] R.N. Patel, S.K. Patel, D. Kumhar, N. Patel, A.K. Patel, R.N. Jadeja, N. Patel, R.J. Butcher, S. Herrero, M. Cortijo, Two new copper(II) binuclear complexes with 2-[(E)-(pyridine-2yl-hydrazono)methyl]phenol: molecular structures, quantum chemical calculations, cryomagnetic properties and catalytic activity, Polyhedron 188 (2020) 114687.
[41] L. Yang, D.R. Powell, R.P. Houser, Structural variation in copper(i) complexes with pyridylmethylamide ligands: structural analysis with a new four-coordinate geometry index, τ4, Dalton Trans. (2007) 955–964.
[42] Y.P. Singh, R.N. Patel, Y. Singh, D. Choquesillo-Lazarte, R.J. Butcher, Classical hydrogen bonding and stacking of chelate rings in new copper(ii) complexes, Dalton Trans. 46 (2017) 2803–2820.
[43] R.N. Patel, Y.P. Singh, Y. Singh, R.J. Butcher, J.P. Jasinski, New di-μ-oxidovanadium(V) complexes with NNO donor Schiff bases: synthesis, crystal structures and electrochemical studies, Polyhedron 133 (2017) 102–109.
[44] K. Nakamoto, Infrared Spectra of Inorganic and Coordination Compounds, fifth ed., Willey, New York, 1997.
[45] H. Okawa, M. Tadokoro, Y. Aratake, M. Ohba, K. Shindo, M. Mitsumi, M. Koikawa, M. Tomono, D.E. Fenton, Dicopper(II, II) and dicopper(I, II) complexes of a series of dinucleating macrocycles, J. Chem. Soc. Dalton Trans. (1993) 253–258.
[46] R.C. Long, D.N. Hendrickson, A stereoselective synthesis of 1,3-diol derivatives and application to the ansa bridge of rifamycin S, J. Am. Chem. Soc. 105 (1983) 1513–1521.
[47] M. Thirumavalavan, P. Akilan, M. Kandaswamy, Synthesis of new macrobicyclic tricompartmental ligands and site preference of metal ion: structural and electrochemical properties of mononuclear copper(II) complexes, Inorg. Chem. Commun. 5 (2002) 422–426.
[48] M. Iqbal, I. Ahmad, S. Ali, N. Muhammad, S. Ahmed, M. Sohail, Dimeric "paddle-wheel" carboxylates of copper(II): synthesis, crystal structure and electrochemical studies, Polyhedron 50 (2013) 524–531.
[49] Y.P. Singh, R.N. Patel, Y. Singh, R.J. Butcher, P.K. Vishwakarma, R.K.B. Bhubon Singh, Structure and antioxidant superoxide dismutase activity of copper(II) hydrazone complexes, Polyhedron 122 (2017) 1–15.
[50] Y. Singh, R.N. Patel, S.K. Patel, A.K. Patel, N. Patel, R. Singh, R.J. Butcher, J.P. Jasinski, A. Gutierrez, Experimental and quantum computational study of two new bridged copper(II) coordination complexes as possible models for antioxidant superoxide dismutase: molecular structures, X-band electron paramagnetic spectra and cryogenic magnetic properties, Polyhedron 171 (2019) 155–171.
[51] B.P. Maurya, M. Ikram, S. Khan, R.J. Singh, S = 12, S = 1 and S = 2 EPR spectra in copper doped KHSO4 single crystal, Solid State Commun. 98 (1996) 843–845.
[52] J.C. Jeffery, J.P. Maher, C.A. Otter, P. Thornton, M.D. Ward, Synthesis of the potentially pentadentate ligand 6,6″-bis(2-hydroxyphenyl)-2,2′:6′,2″- terpyridine (H_2L) and the crystal structure and magnetic properties of $[\{Cu(HL)\}_2][PF_6]_2{\cdot}5MeCN$, J. Chem. Soc. Dalton Trans. (1995) 819–824.
[53] E. Garribba, G. Micera, D. Sanna, L. StrinnaErre, The Cu(II)-2,2′-bipyridine system revisited, Inorg. Chim. Acta. 299 (2000) 253–261.
[54] S. Thakurta, J. Chakraborty, G. Rosair, J. Tercero, M.S. El Fallah, E. Garribba, S. Mitra, Synthesis of two new linear trinuclear Cu(II) complexes: mechanism of magnetic coupling through hybrid B3LYP functional and CShM studies, Inorg. Chem. 47 (2008) 6227–6235.
[55] A.H. Maki, B.R. Mc Garvey, Electron spin resonance in transition metal chelates. I. Copper (II) bis acetylacetonate, J. Chem. Phys. 29 (1958) 35–40.
[56] E.F. Hasty, T.J. Colburn, D.N. Hendrikson, Copper(II) and vanadyl complexes of binucleating ligands. Magnetic exchange interactions propagated through an extensive organic system, Inorg. Chem. 12 (1973) 2414–2421.
[57] R. Klement, F. Stock, H. Elias, H. Paulus, P. Pelikán, M. Valko, M. Mazúr, Copper(II) complexes with derivatives of salen and tetrahydrosalen: a spectroscopic, electrochemical and structural study, Polyhedron 18 (1999) 3617–3628.
[58] K.S. Banua, T. Chattopadhyaya, A. Banerjee, S. Bhattacharya, E. Zangrandoc, D. Das, Catechol oxidase activity of dinuclearcopper(II) complexes of Robson type macrocyclic ligands: syntheses, X-ray crystal structure, spectroscopic characterization of the adducts and kinetic studies, J. Mol. Catal. Chem. 310 (2009) 34–41.
[59] C.T. Yang, M. Vetrichelvan, X. Yang, B. Moubarki, K.S. Murray, J.J. Vittal, Syntheses, structural properties and catecholase activity of copper(ii) complexes with reduced Schiff base N-(2-hydroxybenzyl)-amino acids, Dalton Trans. (2004) 113–121.
[60] S. Albedyhl, M.T. Averbuch-Pouchot, C. Belle, B. Krebs, J.L. Pierre, E. Saint-Aman, S. Torelli, DinuclearZinc(II)−Iron(III) and iron(II)−Iron(III) complexes as models for purple acid phosphatases, Eur. J. Inorg. Chem. 2001 (2001) 1457–1464.
[61] A. Neves, L.M. Rossi, A.J. Bortoluzzi, B. Szpoganicz, C. Wiezbicki, E. Schwingel, Catecholase activity of a series of dicopper(II) complexes with variable Cu-OH(phenol) moieties, Inorg. Chem. 41 (2002) 1788–1794.
[62] K.S. Banu, T. Chattopadhyay, A. Banerjee, S. Bhattacharya, E. Suresh, M. Nethaji, E. Zangrando, D. Das, Catechol oxidase activity of a series of new DinuclearCopper(II) complexes with 3,5-DTBC and TCC as substrates: syntheses, X-ray crystal structures, spectroscopic characterization of the adducts and kinetic studies, Inorg. Chem. 47 (2008) 7083–7093.
[63] C. Beauchamp, I. Fridovich, Superoxide dismutase: improved assays and an assay applicable to acrylamide gels, Anal. Biochem. 44 (1971) 276–287.
[64] H.J. Bielski, G.G. Shiue, B. Bajuk, Reduction of nitro blue tetrazolium by CO2- and O2- radicals, J. Phys. Chem. 84 (1980) 830–833.
[65] Y. Singh, R.N. Patel, S.K. Patel, R.N. Jadeja, A.K. Patel, N. Patel, H. Roy, P. Bhagriya, R. Singh, R.J. Butcher, J.P. Jasinski, S. Herrero, M. Cortijo, Supramolecular assemblies of new pseudohalide end-to-end bridged copper(II) complex and molecular structural variety of Penta and Hexa-coordinated metal(II) complexes with hydrazido-based ligand, Inorg. Chim. Acta. 503 (2020) 119371.
[66] Y. Li, Z.Y. Yang, J.C. Wu, Synthesis, crystal structures, biological activities and fluorescence studies of transition metal complexes with 3-carbaldehyde chromone thiosemicarbazone, Eur. J. Med. Chem. 45 (2010) 5692–5701.
[67] R.N. Patel, Y. Singh, Y.P. Singh, A.K. Patel, N. Patel, R. Singh, R.J. Butcher, J.P. Jasinski, E. Colacio, M.A. Palacios, Varying structural motifs, unusual X-band electron paramagnetic spectra, DFT studies and superoxide dismutase enzymatic activity of copper(ii) complexes with N′-[(E)-phenyl(pyridin-2-yl)methylidene] benzohydrazide, New J. Chem. 42 (2018) 3112–3136.
[68] R.N. Patel, D.K. Patel, V.P. Sondhiya, K.K. Shukla, Y. Singh, A. Kumar, Synthesis, crystal structure and superoxide dismutase activity of two new bis(μ-acetato/μ-nitrato) bridged copper(II) complexes with N′-[phenyl(pyridin-2-yl)methylidene] benzohydrazone, Inorg. Chim. Acta. 405 (2013) 209–217.
[69] V. Pelmenschikov, P.E.M. Siegbahn, Copper−Zinc superoxide dismutase: theoretical insights into the catalytic mechanism, Inorg. Chem. 44 (2005) 3311–3320.

[70] K.S. Banu, T. Chattopadhyay, A. Banerjee, M. Mukherjee, S. Bhattacharya, G.K. Patra, E. Zangrando, D. Das, Mono- and dinuclearmanganese(III) complexes showing efficient catechol oxidase activity: syntheses, characterization and spectroscopic studies, Dalton Trans. (2009) 8755–8764.

[71] Q. Xiang Li, Q. Hui Luo, Y. Zhi Lia, M. Chang Shena, A study on the mimics of Cu–Zn superoxide dismutase with high activity and stability: two copper(II) complexes of 1,4,7- triazacyclononane with benzimidazole groups, Dalton Trans. (2004) 2329–2335.

[72] K.C. Nicolaou, K. Namoto, A. Ritze'n, T. Ulven, M. Shoji, J. Li, G. D'Amico, D. Liotta, C.T. French, M. Wartmann, K.H. Altmann, P. Giannakakou, Chemical synthesis and biological evaluation of cis- and trans-12,13-cyclopropyl and 12,13-cyclobutyl epothilones and related pyridine side chain analogues, J. Am. Chem. Soc. 123 (2001) 9313–9323.